ADVANCED MATERIALS

DOI: 10.1002/adma.200703160

Polarization Engineering of Thermal Radiation Using Metallic Photonic Crystals**

By *Jae-Hwang Lee, Jeffrey Chi Wai Lee, Wai Leung, Ming Li, Kristen Constant, Che Ting Chan,* and *Kai-Ming Ho**

Thermal radiation (TR) from a hot object was one of the clues that led to the development of quantum physics a century ago. Recently it has attracted renewed scientific interest as extraordinary phenomena have been demonstrated for objects patterned periodically on the micrometer scale, for example, coherent TR[1,2] and spectrally enhanced TR.[3–6] While TR has been known to be polarized by fundamental optical phenomena, such as refraction[7] and diffraction,[8] engineering the polarization of TR has been attempted by few.[9,10] Polarization-engineered thermal emitters have the potential to enable higher conversion efficiency in thermophotovoltaics. Here we report that a series of polarized thermal emitters (PTEs) can be selectively enhanced with a high degree of polarization (DOP) up to 0.5 through the use of metallic photonic crystals (MPCs). We show that strong absorption induced by greatly reduced group velocity for a certain polarization is the underlying physical basis for this phenomenon. As the PTEs have two TR channels with different linear polarizations, advanced applications such as tunable multichannel infrared (IR) emitters and encrypted infrared markers are also possible.

Recently we reported that a nickel MPC with only two layers (as in Fig. 1a) has two highly enhanced TR peaks when a homogeneous backplane is added.[11] For this study, we have fabricated two more variations having mutual angles of 60° and 30°, as seen in Figure 1b and c to study polarized TR. We designate the MPCs as 90°, 60°, and 30° MPCs, respectively. Measurements were made using the radiometric setup shown in Figure 1d. The MPC is mounted on a heated copper block in a high vacuum chamber (ca. 10^{-5} Torr (1 Torr = 1.333 × 10^2 Pa)). TR is collected normal to the surface and directed into a Fourier-transform infrared (FT-IR) spectrometer (Magna 760, Nicolet), and then passed through a linear IR polarizer (Spectra-Tech Inc.).

Polarization-dependent TR power is measured at 800 K as a function of the transmission angle of the polarizer from 0° to 180° in 10° steps. To obtain the corresponding emissivities, TR power from a blackbody is also measured under the same conditions. We assume that TR from the blackbody source is completely unpolarized. In the emissivity map of the 90° MPC in Figure 2a, the two major emission peaks in the vicinity of photonic band edge at 3377 cm^{-1} and 2827 cm^{-1}[11] are differently polarized parallel or perpendicular to the rods. We label the peaks with P90a and P90b, where ''a'' and ''b'' represent their family. The third peak, P90c appears far from the photonic band edge, and its emissivity peak is significantly smaller

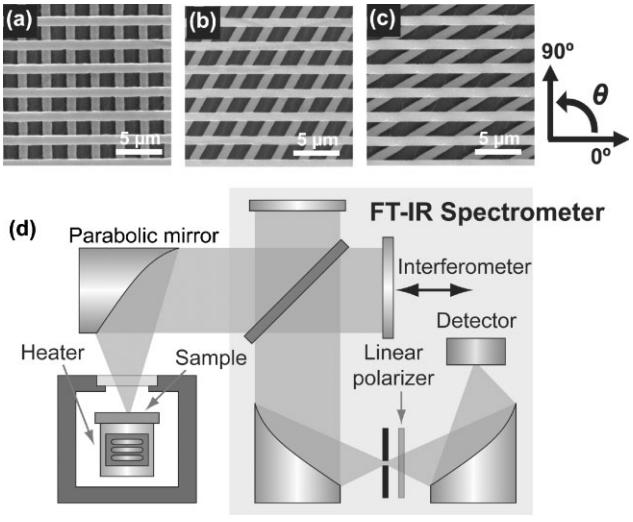

Figure 1. Polarization-dependent thermal radiation measurement. Scanning electron microscopy images of MPCs with different mutual angles of a) 90°, b) 60°, and c) 30° are shown. The distance between the rods is 2.6 μm, and each rod is 1.1 μm wide and 1.2 μm high. The transmission axis of the polarizer is set as zero when it is parallel to the top layer of the rods of the MPCs, as depicted on the far right. d) Schematic illustration of the radiometric setup. The collection angle is perpendicular to the surface with an acceptance angle of 11°. The sampling area is approximately 1 × 1 mm^2.

[*] Prof. K.-M. Ho, Dr. J.-H. Lee, Dr. W. Leung, Dr. M. Li
Ames Laboratory-US DOE and
Department of Physics and Astronomy
Iowa State University
Ames, IA 50011 (USA)
E-mail: kmh@ameslab.gov
J. C. W. Lee, Prof. C. T. Chan
Department of Physics
Hong Kong University of Science and Technology
Clear Water Bay, Hong Kong (PR China)
Prof. K. Constant
Ames Laboratory-US DOE and
Department of Materials Science and Engineering
Iowa State University Ames, IA 50011 (USA)

[**] This work is supported by the Director for Energy Research, Office of Basic Energy Sciences. The Ames Laboratory is operated for the U.S. Department of Energy by Iowa State University under contract No. DE-AC02-07CH11358. J.C.W.L. and C.T.C. acknowledge support from HKRGC grant No. 600403.

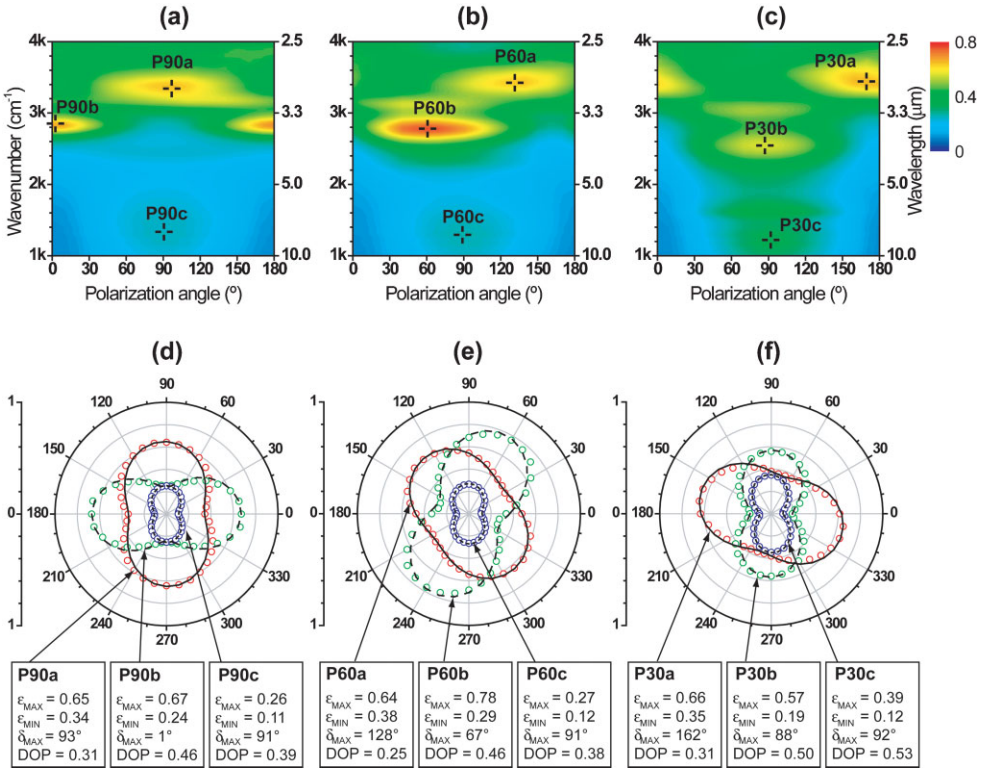

Figure 2. Polarization-dependent emissivities of MPCs. The emissivities of the MPCs with the mutual angles of a) 90°, b) 60°, and c) 30° are color-mapped at the same scale: 0 to 0.8. Polar plots of the three peaks for d) 90°, e) 60°, and f) 30° are shown as colored circles with their fitted curves. The fitting parameters are shown under each label of the peaks. Because the emissivities are measured from 0° to 180°, the values out of the range are extended by the two-fold symmetry. Each radial division is 0.2.

and broader than P90a and P90b. When changing the mutual angle to 60° and 30° successively, which means the bottom layer of each MPC rotates clockwise; the three peaks shift both in polarization angle and in wavelength in Figure 2b and c. Spectroscopically, the peaks in the family ''a'' show a relatively small shift of less than 4% while the other peaks in the groups ''b'' and ''c'' show larger red-shifts up to 11% and 21%, respectively. In addition, we notice that polarization angles of the two major peaks rotate counterclockwise in opposition to the rotation of the bottom layer. For the three selected peaks of each MPC, polarization-dependent emissivities are polar-plotted in Figure 2d–f. By assuming a partial polarization, the measured emissivities are fit with a function of Malus's law,[12] $\varepsilon_{MAX}\cos^2(\theta-\delta_{MAX})+\varepsilon_{MIN}\cos^2(\theta-\delta_{MAX}-90^\circ)$, where ε_{MAX} and ε_{MIN} are the maximum and minimum emissivities at two orthogonal angles, δ_{MAX} and $\delta_{MAX}-90^\circ$, respectively. The fitted curves are co-plotted on the polar plots with their parameters shown below. All the polarization-dependent emissivities are fit by these calculations to an excellent degree, clearly demonstrating that the thermal emission is linearly polarized. From the parameters, we calculate DOP, defined by $(\varepsilon_{MAX}-\varepsilon_{MIN})/(\varepsilon_{MAX}+\varepsilon_{MIN})$. The peaks in family ''b'' show high DOP for all the mutual angles close to 0.5 with high emissivity.

We calculate the absorptance of the MPCs shown in Figure 3 according to Kirchhoff's law: absorptance is directly related to emissivity at equilibrium. Excellent agreement with the experimental emissivity spectra in Figure 2 is demonstrated. Small discrepancies may arise from the fact that the calculation considers only normal incidence while the experiment measures radiation within a finite acceptance angle. We also calculate polarization angles as a function of the mutual angle in Figure 3f, which is also consistent with the experiment. The negative slope of the families ''a'' and ''b'' represents that the rotation directions of the structure and polarization angle are opposite. The different trends of two families imply that the peaks of each family come after different interaction with the structure. To see the origin of the peaks P90a and P90b, in the calculations, we tentatively remove an imaginary part of the complex refractive index of nickel for top and bottom layers while the backplane remains unchanged. As absorption by top and bottom layers becomes zero, P90a almost disappeared, however, P90b still exist with similar absorptance value. From the results, we determine that P90a mainly originates from the enhancement of the intrinsic absorption of nickel in the top and bottom layer while P90b results from the whole structure, including the backplane. The calculated electric field profiles for P90a and P90b in Figure 3d and e show the 90° MPC intensifies the internal electric field 7 to 10 times compared to that on the outside, which suggests that significantly reduced group velocity increases the interaction of light with nickel and enhances the intrinsic absorption. In addition, the difference in the vertical positions of high-electric-field regions of P90a and P90b in Figure 3d and e explains why each peak is affected by different parts of the MPC. For the peaks in family ''c'', it suggests that the top layer of each MPC acts like a metallic wire grid and light can penetrate the layer and be absorbed by an underlying structure if the polarization is perpendicular to the grid. As increasing the height of rods in the top layer in the calculation of 90° MPC, P90c showed a red-shift proportional to the height of rods in the top layer. This may explain qualitatively how the red-shift of the peaks in group ''c'' is caused by reducing the mutual angle: The bottom layer contributes to increase the effective height of the top layer as the bottom layer has a structural component parallel to the top layer for non-orthogonal structures,

ADVANCED MATERIALS

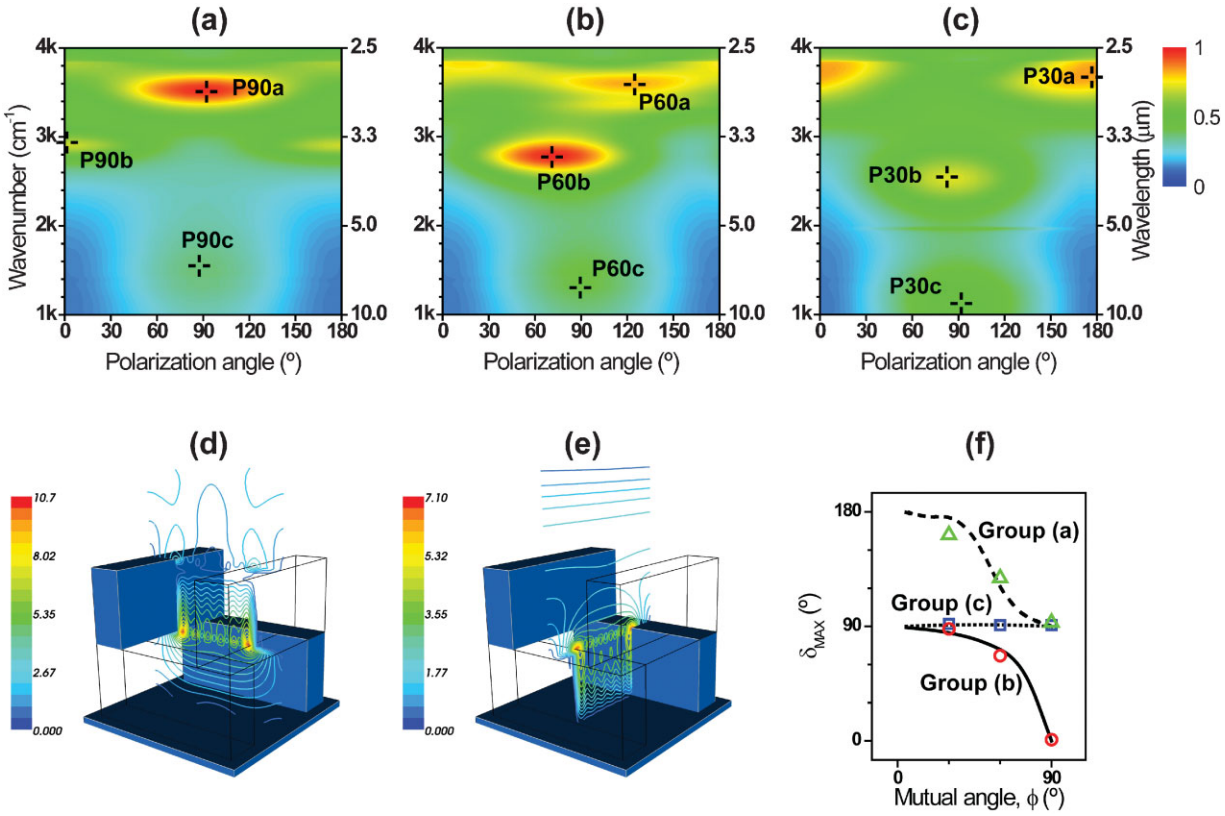

Figure 3. Numerical simulations for the MPCs. Polarization-dependent absorptance spectra of a) 90°, b) 60°, and c) 30° MPCs are calculated and plotted as linear color maps. Peak positions are marked with the same labels as in Figure 2. The profiles of the electric field strength in a unit cell of 90° MPC are shown for d) P90a and e) P90b. The strength is normalized to that of an incoming wave. f) Calculated polarization angles for the peaks as a function of the mutual angle are shown as curves with the measured values as colored marks.

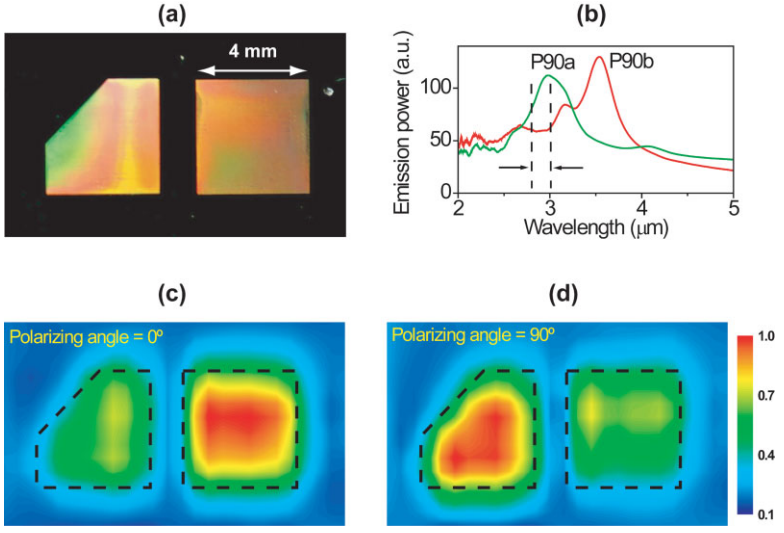

Figure 4. Polarized TR marker made from a 90° MPC. a) Photograph of the marker. The dark area surrounding the MPCs is a flat nickel surface. The left MPC was fabricated to have non-square shape for better discrimination in thermal imaging. b) Spectra of thermal radiation power of the 90°-MPC for the two orthogonal polarization angles at the same temperature of 800 K. The dashed lines show the range of wavelength used for the thermal imaging. TR distribution maps taken at the different polarization angles of c) 0° and d) 90° are shown.

60° and 30° MPC. We note that the radiation behavior of the MPCs can not be simply understood with two wire-grid polarizers and a backplane, mainly because all components are working collectively rather than independently at the photonic band edge.

A thermal marker has been fabricated to demonstrate a potential application. As shown in Figure 4a, this consists of two identical 90° MPCs, one rotated 90° to the other. The high emissivity and DOP of P90a and P90b in Figure 4b allows the wavelength windows around the two major peaks to be utilized in polarized TR applications. At the same temperature, the two patterns are clearly distinguishable in the spatial distribution of TR of Figure 4c and d, which is not possible without a polarizing detector. We can also design a multichannel IR emitter and polarization-selective IR absorbers as the two emission or absorption wavelengths are selectable using an additional polarizer.

We demonstrate that the MPC can enhance TR in the vicinity of its photonic band edge with a preferred polarization. With rigorous calculations, we show that enhanced light-matter interaction resulting from slow group velocity for a given wavelength and polarization is the physics underlying this phenomenon. As the polarized TR does not rely on angle-sensitive phenomena such as refraction or diffraction, it can be used at a wide range of viewing angles and is scalable for different working wavelengths. The tailorability of polarization characteristics of TR makes possible advanced applications using polarized IR sources in sensing, security, and energy science.

Experimental

Optical Measurements: The temperature calibration and radiometric calibration was the same as in our previous report [11]. We used a lab-built blackbody source to secure a radiation angle greater than 11°. The blackbody source was a copper block having a spherical cavity of 100 mm diameter and 10 mm exit opening. The entire inner surface was coated with carbon black and exhibited the same TR power as that of a commercial blackbody source (M335, Mikron Infrared, Inc.). For the thermal images in Figure 4c and d, TR from a sample was collected at different 13×8 points with a spacing of 1 mm, the same as the spatial resolution of the radiometry setup. Acquired TR powers within a given spectral window were averaged and normalized to reconstruct the spatial distribution of TR.

Numerical Simulations: All calculations were based on a planewave-based transfer-scattering matrix method [13, 14]. The absorptance maps in Figure 3a–c are calculated by subtracting calculated reflectance and transmittance from unity. For realistic calculations, experimentally acquired optical constants of nickel [11] were used for the absorptance maps while optical parameters from the Ref. [15] were used for the electric field profiles in Figure 3d and e. The curves of polarization angles in Figure 3f were acquired by calculations of a series of two-layer nickel structures having mutual angles from 5° to 90° with a 5° step.

Received: December 19, 2007
Revised: February 21, 2008

[1] J.-J. Greffet, R. Carminati, K. Joulain, J.-P. Mulet, S. Mainguy, Y. Chen, *Nature* **2002**, *416*, 61.
[2] M. Laroche, R. Carminati, J.-J. Greffet, *Phys. Rev. Lett.* **2006**, *96*, 123903.
[3] M. U. Pralle, N. Moelders, M. P. McNeal, I. Puscasu, A. C. Greenwald, J. T. Daly, E. A. Johnson, T. George, D. S. Choi, I. El-Kady, R. Biswas, *Appl. Phys. Lett.* **2002**, *81*, 4685.
[4] S.-Y. Lin, J. G. Fleming, I. El-Kady, *Appl. Phys. Lett.* **2003**, *83*, 593.
[5] S. Enoch, J.-J. Simon, L. Escoubas, Z. Elalmy, F. Lemarquis, P. Torchio, G. Albrand, *Appl. Phys. Lett.* **2005**, *86*, 261101.
[6] S. Y. Lin, J. G. Fleming, I. El-Kady, *Opt. Lett.* **2003**, *28*, 1683.
[7] A. G. Worthing, *J. Opt. Soc. Am.* **1926**, *13*, 635.
[8] W. Ohman, *Nature* **1961**, *192*, 254.
[9] P. J. Hesketh, J. N. Zemel, B. Gebhart, *Phys. Rev. B* **1988**, *37*, 10795.
[10] S. Ingvarsson, L. J. Klein, Y.-Y. Au, J. A. Lacey, H. F. Hamann, *Opt. Lett.* **2007**, *15*, 11249.
[11] J.-H. Lee, Y.-S. Kim, K. Constant, K.-M. Ho, *Adv. Mater.* **2007**, *19*, 791.
[12] E. Hecht, *Optics*, 4th ed. Addison-Wesley, San Francisco, CA **2002**.
[13] J. B. Pendry, *J. Mod. Opt.* **1994**, *41*, 209.
[14] Z.-Y. Li, L.-L. Lin, *Phys. Rev. E* **2003**, *67*, 046607.
[15] D. W. Lynch, W. R. Hunter, in: *Handbook of Optical Constants of Solid*, E. D. Palik), Academic, London **1985**.